Bone marrow mesenchymal stem cell-derived exosomes protect podocytes from HBx-induced ferroptosis

Xiaoqian Yang [Equal first author, 1], Yani Yu [Equal first author, 1], Baoshuang Li [1], Yueqi Chen [1], Moxuan Feng [1], Yongzheng Hu [1], Wei Jiang [Corresp. 1]

[1] Department of Nephrology, The Affiliated Hospital of Qingdao University, Qingdao, China

Corresponding Author: Wei Jiang
Email address: jiangwei866@qdu.edu.cn

Introduction. Hepatitis B virus-associated glomerulonephritis (HBV-GN) is a common secondary kidney disease in China, the pathogenesis of which is not completely clear, and there is still a lack of effective treatment. **Methods**. The mechanism of exosomes derived from bone marrow mesenchymal stem cells (BMSCs) was investigated by using HBx-transfected human renal podocytes. Cell viability was detected by CCK8 assay. Iron and malondialdehyde (MDA) contents were detected by using commercial kits. Reactive oxygen species (ROS) levels were measured by flow cytometry analysis. The expression of ferroptosis related molecules was detected by quantitative real-time polymerase chain reaction (qRT-PCR) and Western blot. The effect of miR-223-3p transferred by BMSC-derived exosomes on HBx-overexpressing podocytes was proved by using miR-223-3p inhibitor. **Results**. The cell viability of podocytes reduced at 72h or 96h after the transfection of lentivirus overexpressing HBx protein ($p<0.05$). Ferroptosis-related proteins, including glutathione peroxidase 4 (GPX4) and solute carrier family 7 member 11 (SLC7A11) were down-regulated upon HBx overexpression, while acyl-CoA synthetase long-chain family member 4 (ACSL4) was up-regulated ($p<0.05$). And intracellular levels of iron, MDA, and ROS were also enhanced ($p<0.05$). BMSC-derived exosomes protected against ferroptosis induced by HBx overexpression in podocytes. miR-223-3p was enriched in BMSC-derived exosomes. Application of miR-223-3p inhibitor reversed the protective effect of BMSC-derived exosomes on HBx-induced ferroptosis in podocytes. **Conclusion**. BMSC-derived exosomes inhibit HBx-induced podocyte ferroptosis by transferring miR-223-3p.

1 # Bone marrow mesenchymal stem cell-derived exosomes

2 # protect podocytes from HBx-induced ferroptosis

4 Xiaoqian Yang[1]¶, Yani Yu[1]¶, Baoshuang Li[1], Yueqi Chen[1], Moxuan Feng[1], Yongzheng Hu[1], Wei

5 Jiang[1]

7 [1] Department of Nephrology, The Affiliated Hospital of Qingdao University, Qingdao, China

9 Corresponding Author:

10 Wei Jiang[1]

11 No.16 Jiangsu Road, Qingdao, 266003, China

12 Email address: jiangwei866@qdu.edu.cn

14 ¶These authors contributed equally to this study.

17 **Abstract**

18 **Introduction**. Hepatitis B virus-associated glomerulonephritis (HBV-GN) is a common secondary

19 kidney disease in China, the pathogenesis of which is not completely clear, and there is still a lack

20 of effective treatment.

21 **Methods**. The mechanism of exosomes derived from bone marrow mesenchymal stem cells

22   (BMSCs) was investigated by using HBx-transfected human renal podocytes. Cell viability was

23   detected by CCK8 assay. Iron and malondialdehyde (MDA) contents were detected by using

24   commercial kits. Reactive oxygen species (ROS) levels were measured by flow cytometry

25   analysis. The expression of ferroptosis related molecules was detected by quantitative real-time

26   polymerase chain reaction (qRT-PCR) and Western blot. The effect of miR-223-3p transferred by

27   BMSC-derived exosomes on HBx-overexpressing podocytes was proved by using miR-223-3p

28   inhibitor.

29   **Results**. The cell viability of podocytes reduced at 72h or 96h after the transfection of lentivirus

30   overexpressing HBx protein ($p<0.05$). Ferroptosis-related proteins, including glutathione

31   peroxidase 4 (GPX4) and solute carrier family 7 member 11 (SLC7A11) were down-regulated

32   upon HBx overexpression, while acyl-CoA synthetase long-chain family member 4 (ACSL4) was

33   up-regulated ($p<0.05$). And intracellular levels of iron, MDA, and ROS were also enhanced

34   ($p<0.05$). BMSC-derived exosomes protected against ferroptosis induced by HBx overexpression

35   in podocytes. miR-223-3p was enriched in BMSC-derived exosomes. Application of miR-223-3p

36   inhibitor reversed the protective effect of BMSC-derived exosomes on HBx-induced ferroptosis

37   in podocytes.

38   **Conclusion**. BMSC-derived exosomes inhibit HBx-induced podocyte ferroptosis by transferring

39   miR-223-3p.

40

41   ## Introduction

42   Hepatitis B virus-associated glomerulonephritis (HBV-GN) remains a huge healthcare burden

43   worldwide, although the prevalence of hepatitis B virus (HBV) infection has declined due to the

44   vaccination policy (Hu et al. 2020; Liu et al. 2020). The prevalence of chronic HBV infection was

45   4.1% globally and 7.8% in China (Collaborators 2022). Among those patients in China, about 6.8-

46   20% may progress into HBV-GN (Liu et al. 2020). And it is a common secondary renal disease in

47   most developing countries including China (Yang et al. 2019). The most frequent subtype is

48   membranous nephropathy (MN) which usually presents with nephrotic syndrome clinically (Hu et

49   al. 2020). Some patients may develop mild to moderate proteinuria accompanied by hematuria,

50   and finally progress to end-stage of renal disease (ESRD). HBx as a multifunctional protein

51   encoded by HBV can modulate multiple signaling pathways such as HBV replication, cellular

52   transcription, cell cycle, DNA repair, etc (Lei et al. 2019; Yang et al. 2018). Past studies have

53   shown that mutations at key genetic loci plays an important role in HBV-GN progression (Hui et

54   al. 2014). HBx overexpression could decrease cell viability of podocytes and cause increased

55   podocyte injury (Lei et al. 2019). Podocytes function as an essential component of glomerular

56   filtration barrier, whose impairment leads to proteinuria, while a reduced number of podocytes is

57   considered to be a relative risk factor for progressive renal impairment (He et al. 2017). Thus, we

58   consider that podocytes injury induced by HBx overexpression may be an important pathological

59   process in the development of HBV-GN, however the exact molecular mechanism remains

60   unclear.

61

62   Ferroptosis is a form of programmed cell death characterized by iron dependence and

63   accumulation of lipid peroxides (Li et al. 2020a; Xu et al. 2021). Excessive iron produces a large

64 number of reactive oxygen species (ROS) via lipid peroxidase or non-enzymatic free radical

65 reaction, which can synthesize lipid peroxides together with unsaturated fatty acids of lipid

66 membranes, leading to membrane damage and cell death (Xu et al. 2021). Studies have found that

67 increased lipid peroxides in podocytes cultured with high glucose could induce ferroptosis in

68 podocytes (Wu et al. 2022b). Ferroptosis inhibitors could remarkably reduce iron content in high

69 fructose-cultured podocytes, inhibit podocyte ferroptosis and alleviate diabetic kidney damage

70 (Zhang et al. 2021). Therefore, we speculate that podocyte ferroptosis may play an essential role

71 in renal disease pathogenesis, while restraining podocyte ferroptosis could slow the progression of

72 kidney disease. Recent studies have shown that elevated level of iron in hepatocytes due to HBx

73 overexpression could induce hepatocyte ferroptosis of acute liver failure by triggering lipid

74 peroxidation (Liu et al. 2021a). However, the underlying mechanism by which ferroptosis acts

75 during the development of HBV-GN requires clarification.

76

77 Mesenchymal stem cells (MSCs) are a kind of pluripotent stem cells that possess multiple

78 differentiation potentials (Nikfarjam et al. 2020). It has been shown that MSCs could be used to

79 treat kidney disease, and the key lies in releasing extracellular vesicles (EVs) via paracrine(Bochon

80 et al. 2019; Wu et al. 2022a). Exosomes are one of the main subpopulations of EVs, containing a

81 wide variety of proteins and miRNAs that take part in regulating numerous physiological and

82 pathological processes (Lin et al. 2022). Previous studies have found that the injection of exosomes

83 derived from bone marrow mesenchymal stem cells (BMSCs) into diabetic nephropathy rats can

84 significantly improve the oxidative stress injury of renal tissue, reduce the discharge of urine

85 protein and protect kidney function (Mao et al. 2021). This indicates that the exosomes are

86 important for MSCs' protective role in the treatment of kidney disease. In addition, recent studies

87 found that MSC-derived exosomes are also involved in the regulation of ferroptosis (Lin et al.

88 2022). Increasing evidence have revealed that exosomal miRNA cargo is largely responsible for

89 the protective effects of these exosomes (Ding et al. 2020; Yi & Tang 2021). MiR-223-3p is one

90 of the most abundant miRNAs in BMSCs (Zhao et al. 2020). Lu *et al* found that MSC-derived

91 exosomes could alleviate liver injury in acute liver failure rats by delivering miR-223-3p (Lu et al.

92 2019). It has also been reported that the deficiency of miR-223 may be closely related to the

93 exacerbation of lupus nephritis (Hiramatsu-Asano et al. 2020). This suggests exosomal miR-223-

94 3p is critical to tissue injury improvement. However, the practical effect of BMSC-derived

95 exosomes and its miRNAs on podocyte injury in HBV-GN are still unclear. In this study, we

96 hypothesize that BMSC-derived exosomes are key regulatory factors in the pathogenesis of HBV-

97 GN by regulating podocyte ferroptosis, in which miR-223-3p plays a vital role. This study may

98 provide a new direction for the cognition and treatment of HBV-GN.

99

100

101 **Materials and Methods**

102 **Cell culture and transfection**

103 Human renal podocytes were obtained from BeNa Culture Collection (Henan, China), and were

104 cultured in Dulbecco's Modified Eagle Medium (DMEM) containing 10% fetal calf serum at 37℃

105 with $5\%CO_2$, and saturated humidity. Negative control lentivirus (lenti-NC), HBx overexpression

106   lentivirus (lenti-HBx), and miRNA inhibitor were synthesized by Bioogenetech (Anhui, China).

107   Podocytes were inoculated on 6-well plates at $5*10^4$ cells/cm^2. When reached 70% confluence,

108   those podocytes were transfected with negative control lentivirus (lenti-NC), HBx overexpressed

109   lentivirus (lenti-HBx), or nothing (control) according to the manufacturer's protocol. The partial

110   experimental groups were as follows: the control group, lenti-NC group, lenti-HBx group.

111   Following transfection of podocytes for 72h, the cells were observed by inverted fluorescence

112   microscopy system (NSHOT) and measured the efficiency of lentivirus transfection into target

113   cells.

114   In the exosome experiment, podocytes were treated with exosomes with protein concentration of

115   0.4μg/μL for 48h after lentivirus transfection. In the miR-223-3p inhibitor experiment,

116   lipofectamine 2000 (Invitrogen) was used to transfect podocytes. In brief, after treated with

117   exosomes, cells were inoculated into 6-well plates for culture, when reached 50% degree of fusion,

118   the cells were transfected with 5μL of inhibitor NC or miR-223-3p inhibitor for 48 h. The

119   transfection efficiency was examined using qRT-PCR. miR-223-3p inhibitor incorporates the

120   reverse complementary synthetic target sites specific binding those target miRNAs and are

121   specially modified, making miRNAs unavailable for normal function.

122

123   **CCK-8 assay**

124   Cell viability was detected by Cell Counting Kit-8 assay. Briefly, differently treated podocytes

125   were inoculated into 96-well plates at 3000 cells/well. Then, 10uL CCK-8 reagent (Servicebio,

126   Wuhan, Hubei, China) was added to each well and incubated for 2h. Each well's optical density

127   (OD) at 450 nm was detected by a microplate reader (Thermo Fisher Scientific, Shanghai, China)

128   to reflect the cell viability.

129

130   **Measurement of MDA and iron**

131   Cells from each group were collected and then centrifuged to remove floating cells and cell

132   fragments. After the cells were broken up by ultrasound treatment and subjected to centrifugation

133   to obtain the supernatant. Protein concentration was determined using BCA Assay Kit (Beyotime,

134   Biotechnology, Shanghai, China). Malondialdehyde (MDA) quantification was performed using

135   MDA Assay Kit (Sinovac Biotech, Beijing, China) according to the manufacturer's instructions.

136   Briefly, 200μL sample or distilled water was incubated with an MDA reagent for 60min at 100℃.

137   After cooled and centrifuging, the absorbance was measured at 532nm and 600nm with a

138   spectrophotometer for calculating MDA content. Similarly, Fe quantification was performed using

139   Fe Assay Kit (Solarbio, Beijing, China) according to the manufacturer's instructions. 400μL

140   sample or standard or distilled water was incubated with Fe reagent for 5min at 100℃. After

141   mixing with 200μL chloroform and centrifuged, the absorbance was measured at 532nm and

142   600nm with a spectrophotometer for calculating Fe content.

143

144   **Flow cytometry analysis**

145   Reactive oxygen species (ROS) were detected by flow cytometry analysis. According to the

146   manufacturer's protocol of ROS Assay Kit (Meilunbio, Dalian, Liaoning, China, cat.No.

147   MA0219), podocytes of each group were incubated with 10μmol/L DCFH-DA probe or PBS for

148 60min at 37℃. The cell suspension was collected and centrifuged at 1000rpm/min for 5min. After

149 washing and centrifuging with PBS, cell precipitates were collected. Finally, the mean

150 fluorescence intensity of each group was detected using a flow cytometer (Agilent, Beijing, China)

151 to reflect the corresponding ROS level.

152

153 **Western blot**

154 Protein exacted from podocytes were prepared in RIPA lysis buffer (Boster Biological

155 Technology, Wuhan, Hubei, China), and was estimated using BCA protein assay kit (Beyotime).

156 Proteins were separated by SDS-PAGE (G2003, Servicebio), transferred onto PDVF membranes

157 (Millipore) after electrophoresis, and blocked by 5% skimmed milk at room temperature for 1h.

158 After incubation with primary antibodies at 4℃ overnight, the membranes were incubated with

159 secondary antibodies. We quantified the band area using AlphaEase FC software (Alpha Innotech)

160 to reflect the relative expression of target proteins. The results were corrected to the band intensity

161 of GAPDH. The antibodies used are shown in Table 1.

162

163 **qRT-PCR**

164 Total RNAs were isolated from podocytes using TRIzol reagent (Cwbio, Jiangsu, China). Reverse

165 transcription was conducted using Evo-M-MLV Reverse Transcriptase (Accurate Biology, Hunan,

166 China). Subsequently, qPCR reaction was performed using SYBR Green Pro Taq HS premixed

167 qPCR Kit (Accurate Biology) according to the manufacturer's instructions, while the annealing

168 temperature of the primers was set at 60℃. GAPDH served as an internal control. The relative

169   expression of target genes was calculated using the $2^{-\Delta\Delta Ct}$ method and normalized by GAPDH

170   expression. The primer sequences used are shown in Table2. The primer sequence of miR-223-3p

171   was provided by Ribobio (Guangzhou, China), and U6 served as its internal control.

172

173   **Isolation and characterization of BMSC-Derived Exosomes**

174   Mouse bone marrow-derived MSCs were purchased from Procell (Wuhan, Hubei, China) and

175   incubated in DMEM without fetal bovine serum (FBS), but with 10% fetal calf serum at 37℃ with

176   $5\%CO_2$ and saturated humidity. After reaching 70% confluence, the culture medium was

177   centrifuged at 2000×g at 4℃ for 30min, and then filtered. The filtrate was centrifuged twice at

178   100000×g at 4℃ for 70min to remove floating cells and cell fragments, and stored at -80℃. 10μL

179   exosome suspension drops were added for precipitation, and 3% phosphotungstic acid was added

180   for stain. Scattering light analysis performed by NanoFCM particle size analyzer (Xiamen, Fujian,

181   China) was used to measure the size of the collected exosomes. The morphology of exosomes was

182   observed using the transmission electron microscope (Hitachi, Japan). Exosomes were dissolved

183   in radioimmunoprecipitation assay buffer and quantified using BCA Assay Kit (Beyotime). CD9,

184   TSG101, and Calnexin detected by Western blotting were also used to identify the collected

185   exosomes. Using 293T cell lysate as positive control to eliminate experimental operation

186   problems. The antibodies used are shown in Table 1.

187

188   **Uptake test of BMSC-Derived Exosomes**

189   To determine the uptake of BMSC-derived exosomes by human podocytes, exosomes were labeled

190   with red fluorescent dye PKH26 (Umibio, Shanghai, China) and incubated with podocytes in an

191   incubator for 2h, 6h and 24h. Following PBS rinsing, cells were fixed with 4% paraformaldehyde

192   for 30min, washed with PBS, and then stained with 4′,6-diamidino-2-phenylindole. The

193   differential interference contrast (DIC) microscopy image and fluorescence microscopy image

194   were taken by Leica SP8 confocal microscope (Leica Microsystems). And the exosome uptake

195   efficiency was expressed by the proportion of PKH26-positive podocytes at 2h, 6h and 24h.

196

197   **Statistical analysis**

198   Data analysis was performed using GraphPad Prism 9.0 software (GraphPad Software, Inc., La

199   Jolla, CA, USA). All data were expressed as mean ± standard deviation. Data among groups were

200   compared using Student's t-test or one-way ANOVA. $p<0.05$ was deemed statistically significant.

201

202   **Results**

203   **1.   HBx overexpression induced podocytes ferroptosis.**

204   To study the mechanism of HBx-induced podocyte injury, we transfected human renal podocytes

205   with HBx-overexpressed lentivirus and two control groups were set. Cell viability was detected

206   using CCK-8 assay at 24h, 48h, 72h, and 96h, respectively. As shown in Fig 1A, compared with

207   control groups, the cell viability of human renal podocytes significantly decreased at 72h (p=0.049)

208   or 96h (p=0.020) after the transfection of HBx-overexpressed lentivirus. Then, we detected the

209   effect of HBx overexpression on ferroptosis via assessing the lipid peroxidation product MDA and

210   iron levels after lentivirus transfection for 72h. As presented in Fig 1B and C, HBx remarkably

211 increased the intracellular concentration of MDA ($p=0.012$) and iron ($p=0.009$) compared to that

212 of the control cells. Flow cytometry was used to examine the reactive oxygen species generation

213 (Fig 1D). The results revealed that compared with either control or lenti-NC group, the level of

214 ROS was significantly upregulated in lenti-HBx group ($p<0.001$). Finally, the expression of

215 ferroptosis-related molecules glutathione peroxidase 4 (GPX4), acyl-CoA synthetase long-chain

216 family member 4 (ACSL4), and solute carrier family 7 member 11 (SLC7A11) were detected by

217 Western blot and qRT-PCR (Fig 1E, F). The results indicated that HBx reduced GPX4 (p_{western}

218 $_{\text{blot}}=0.011$; $p_{\text{qRT-PCR}}=0.002$) and SLC7A11 ($p_{\text{western blot}}=0.023$; $p_{\text{qRT-PCR}}<0.001$), but induced ACSL4

219 ($p_{\text{western blot}}=0.022$; $p_{\text{qRT-PCR}}=0.001$) expression at both protein and mRNA levels. These findings

220 suggested that HBx triggers ferroptosis in podocytes.

221

222 **2.   Characterization of exosomes isolated from BMSCs.**

223 To better elucidate the effect of exosomes on podocyte injury, exosomes were isolated from

224 BMSCs. Firstly, exosomes were observed as cup-shaped or spherical vesicles enveloped with lipid

225 bilayer under transmission electron microscope (Fig 2A). Next, scattering light analysis indicated

226 that exosomes ranged in diameter from 30 to 150nm, and the mean diameter was 78.41nm (Fig

227 2B). Finally, Western blot analysis of exosomal surface markers verified the expression of TSG101

228 and CD9, whereas calnexin was absent (Fig 2C). These results indicated the successful isolation

229 of exosomes from BMSCs.

230

231 **3.   BMSC-derived exosomes inhibited podocyte ferroptosis induced by HBx.**

232   The ability of human renal podocytes to internalize exosomes from BMSCs was assessed using

233   red fluorescence (PKH26) labeled exosomes. The presence of red fluorescence in podocytes

234   indicated that podocytes were able to internalize BMSC-derived exosomes (Fig 3A). This provided

235   the basis for the action of exosomes in podocytes. We also found that the exosome uptake

236   efficiency by podocyte increased in a time-dependent manner, which reached 100% at 24h. After

237   HBx-induced cell ferroptosis, podocytes were co-incubated with BMSC-derived exosomes. The

238   results showed that cotreatment with HBx and exosomes improved the cell viability of podocytes

239   at 72h (p=0.001) or 96h (p<0.001) in comparison with HBx treatment alone (Fig 3B). Then the

240   detection of ferroptosis-related markers (Fig 3C and D) indicated that cotreatment of HBx and

241   exosomes reduced the content of Fe (p=0.010) and MDA (p=0.070) in podocytes versus the lenti-

242   HBx group. Flow cytometry (Fig 3E) suggested that exosome treatment could significantly lower

243   the ROS level in podocytes transfected with HBx (p<0.001). Western blot analysis was used to

244   detect the expression of ferroptosis-related proteins in podocytes (Fig 3F). The results suggested

245   the cotreatment of HBx and exosomes could increase the expression of GPX4 (p=0.018) and

246   SLC7A11(p<0.001), but decrease the expression of ACSL4 (p=0.030) at the protein level. Also,

247   qRT-PCR detection (Fig 3G) found the expression of these molecules at mRNA level appearing

248   the same trend (p_{GPX4}=0.004, $p_{SLC7A11}$<0.001, p_{ACSL4}<0.001). Taken together, these data

249   demonstrated that exosomes from BMSCs are capable of suppressing HBx-induced ferroptosis of

250   podocytes.

251

252   **4. Exosomes from BMSCs delivered miR-223-3p to suppress HBx-induced ferroptosis in**

253   **podocytes.**

254   The expression of miR-223-3p in HBx-induced podocytes was measured by qRT-PCR after

255   treatment with BMSC-derived exosomes. miR-223-3p expression was obviously lower after

256   induction with HBx than the control group ($p<0.001$), but it was significantly increased by the

257   addition of BMSC-derived exosomes containing miR-223-3p ($p=0.009$). To further determine the

258   effect of miR-223-3p transferred by BMSC-derived exosomes on HBx-overexpressing podocytes,

259   HBx-overexpressing podocytes were transfected with miR-223-3p inhibitor. It seemed that

260   treatment with miR-223-3p inhibitor caused a decline ($p=0.001$) in miR-223-3p expression (Fig

261   4A). Next, the CCK8 assay (Fig 4B) illustrated that the treatment with BMSC-derived exosomes

262   and miR-223-3p inhibitor remarkably attenuated cell viability of podocytes at 72h ($p<0.001$) or

263   96h ($p<0.001$). And the treatment with miR-223-3p inhibitor reversed the downregulation of iron

264   ($p<0.001$), MDA ($p<0.001$), and ROS ($p<0.001$) in HBx-overexpressing podocytes mediated by

265   BMSC-derived exosomes (Fig 4C-F). In addition, qRT-PCR and Western blot analysis (Fig 4G

266   and H) revealed that miR-223-3p inhibitor weakened the effects of BMSC-derived exosomes on

267   GPX4 ($p_{western\ blot}<0.001$, $p_{qRT-PCR}=0.003$) and ACSL4 ($p_{western\ blot}<0.001$, $p_{qRT-PCR}<0.001$)

268   expression at both protein and mRNA levels. However, though the treatment with miR-223-3p

269   inhibitor attenuated the upregulation of SLC7A11 expression caused by BMSC-derived exosomes

270   at the protein level ($p<0.001$), no significant statistical difference was observed at the mRNA level

271   ($p=0.107$). Collectively, these results indicated that delivery of miR-223-3p into podocytes by

272   BMSC-derived exosomes suppressed HBx-induced ferroptosis.

273

274 **Discussion**

275 HBV-GN has been identified as the most common extrahepatic lesion caused by HBV infection

276 (Yang et al. 2019). Podocyte injury may be an important factor in the pathogenesis of HBV-GN

277 (He et al. 2017; Lei et al. 2019). In this study, we found that ferroptosis played a critical role in

278 HBx-induced podocyte injury. In addition, we also found that BMSC-derived exosomes inhibited

279 HBx-induced podocyte ferroptosis through miR-223-3p.

280

281 Ferroptosis is identified as a form of regulated cell death that depends on iron metabolism and lipid

282 peroxidation (Xu et al. 2021). Studies have suggested that ferroptosis was related to the

283 pathogenesis of multiple renal diseases, including acute kidney injury (AKI) and chronic kidney

284 diseases such as diabetic nephropathy (Guan et al. 2021; Mishima et al. 2020). Iron-dependent

285 ROS accumulation is considered to be a trigger of ferroptosis: excessive iron activates the lipid

286 peroxidation chain reaction by participating in the generation of ROS to produce massive lipid

287 peroxides, which result in membrane damage and cell death (Kajarabille & Latunde-Dada 2019).

288 Thus, iron and lipid ROS levels can be used to evaluate the presence of ferroptosis.

289 Malondialdehyde (MDA), as a common by-product of lipid peroxidation, allows the measurement

290 of lipid peroxidation (Xu et al. 2021). The level of MDA was found to raise in folic acid-induced

291 AKI mice kidney tissue (Wang et al. 2021). Similarly, the level of ROS improved in renal tubular

292 epithelial cells of mice with AKI caused by ischemia-reperfusion injury, which indicated that

293 ferroptosis contributed significantly to the process of renal tubular necrosis in AKI (Wang et al.

294 2021). Zhang *et al* found that high glucose-induced ferroptosis of podocytes, which was

295 manifested as increased levels of iron, ROS, and MDA (Zhang et al. 2021). The study also proved

296 that ferroptosis activator erastin reduced podocyte viability. HBx can elevate intracellular ROS

297 levels and participate in mitochondrial oxidative stress (Li et al. 2022). Recent studies supported

298 the critical role of mitochondrial oxidative stress in ferroptosis (Gan 2021). In this study, we found

299 that the viability of podocytes transfected with HBx at 72h or 96h was markedly lower than the

300 two control groups, though there was no significant difference in cell viability between

301 experimental groups at 24h or 48h. Furthermore, the overexpression of HBx obviously enhanced

302 the levels of iron, MDA, and ROS in podocytes. Researchers have found that ACSL4 was also

303 involved in the lipid peroxidation of polyunsaturated fatty acids by generating acyl-CoA (Cui et

304 al. 2021). Normally GPX4 is capable of metabolizing lipid peroxides to non-toxic lipid alcohols

305 at the expense of glutathione (GSH) (Xu et al. 2021). The biosynthesis of important intracellular

306 antioxidant GSH requires the participation of cysteine, which is produced from cystine transported

307 by the cell surface cystine/glutamate antiporter system X_c^- (Li et al. 2020a). SLC7A11 is the active

308 subunit of system X_c^-. Regulating the expression of SLC7A11 will affect the uptake of cystine,

309 leading to the depletion of GSH and ferroptosis (Wu et al. 2022b). Researchers found that the level

310 of GSH as well as the expression of GPX4 and SLC7A11 have decreased during podocyte

311 ferroptosis induced by high fructose (Wu et al. 2022b). Similarly, another research detected that

312 high glucose-induced podocyte ferroptosis, decreased cellular GPX4, and increased ROS content

313 and ACSL4 expression in diabetic nephropathy (Jin et al. 2022). In acute liver failure, HBx induced

314 hepatocyte ferroptosis by activating the SLC7A11 inhibition pathway to weaken the expression of

315 SLC7A11, GSH, and GPX4, and to potentiate intracellular iron deposition (Liu et al. 2021a).

316 Interestingly, Kuo *et al* found that HBx could inhibit hepatic stellate cell ferroptosis and lead to

317 liver fibrosis (Kuo et al. 2020). In this study, we found that overexpression of HBx in podocytes

318 downregulated the expression of antioxidant GPX4 and SLC7A11, but upregulated the expression

319 of ACSL4 which was related to lipid oxidation. These findings verify the crucial role of HBx-

320 induced podocyte ferroptosis in HBV-GN.

321

322 At present, antivirus therapy has been the backbone of HBV-GN treatment due to its efficacy in

323 HBV clearance and proteinuria remission, but fails to improve the glomerular filtration rate (Fu et

324 al. 2020). Therefore, there is an urgent need for more effective treatments to reduce the occurrence

325 and progression of HBV-GN. MSCs can be isolated from adult tissues including bone marrow,

326 adipose tissue, umbilical cord blood, and amniotic fluid, which are easy to obtain and considered

327 an ideal choice for cell therapy (Nikfarjam et al. 2020). Research have proved that most of the

328 MSC-related beneficial effects can be attributed to the effectiveness of released exosomes.

329 Whereas, compared with cell treatment, exosomes have better plasticity which means we can

330 obtain effective target products through exogenous modification (Wu et al. 2022a). Moreover,

331 embolism, tumor proliferation, immune response, and other risks can be avoided (Lu et al. 2019;

332 Wu et al. 2022a).Currently, MSC-derived exosomes have been demonstrated to play similar

333 therapeutic effects as ferroptosis inhibitor Fer-1 in regulating lipid ROS accumulation and

334 ferroptosis-related gene expression (Lin et al. 2022). For instance, MSC-derived exosomes

335 significantly attenuated CCl_4-induced lipid peroxidation in hepatocytes, which is manifested by

336 reduced MDA and lipid ROS in cells, and added SLC7A11 expression (Lin et al. 2022). Exosomes

337 produced by MSCs can reduce the content of MDA in ischemia-reperfusion kidney tissue, increase

338 the level of antioxidant enzyme SOD, and reverse the decline of podocyte viability induced by

339 high glucose(Jin et al. 2019; Li et al. 2020b). Our study manifested that BMSC-derived exosomes

340 significantly attenuated HBx-provoked lipid peroxidation, as manifested by the levels of MDA

341 and ROS in podocytes, and improved podocyte viability. Moreover, BMSC-derived exosomes also

342 abolished other ferroptosis biomarkers raised by HBx overexpression, including decreased

343 expression of GPX4 and SLC7A11 and increased expression of ACSL4. Zhang *et al* found that

344 extracellular vesicles derived from MSCs activated the Nrf2/ARE pathway to upregulate the level

345 of antioxidant enzymes, and reduce the level of oxidative stress damage factor MDA, thus

346 achieving renal injury improvement (Zhang et al. 2016). This was consistent with our findings.

347 Thus, it could be concluded that BMSC-derived exosomes effectively alleviate HBx-induced

348 podocyte ferroptosis.

349

350 As we all known, the functional significance of exosomes is largely lie in its content: miRNAs,

351 mRNAs and proteins. As the most important exosomal component, miRNAs can be selectively

352 encased into exosomes and be involved in the regulation of ferroptosis. Ding *et al* found that

353 ischemia-reperfusion injury induced the upregulation of miR-182-5p and miR-378a-3p, and

354 activated renal ferroptosis by downregulating GPX4 and SLC7A11 (Ding et al. 2020). Human

355 umbilical cord MSC-derived exosomes inhibited the deposition of iron and MDA in

356 cardiomyocytes by carrying miR-23a-3p to protect cardiomyocytes from ferroptosis induced by

357 ischemia-reperfusion (Song et al. 2021). Previous studies have found that miR-223-3p is highly

358 encapsulated in exosomes released from BMSCs, which was also proved by our study (Zhao et al.

359 2020). miR-223-3p can reduce brain ischemia-reperfusion injury by inhibiting inflammatory

360 response, and also promote uterine endothelial angiogenesis to repair acute uterine injury(Liu et

361 al. 2021b; Zhao et al. 2020). In our study, we revealed that miR-223-3p delivered from BMSC-

362 derived exosomes to podocytes suppressed podocyte ferroptosis and restored podocyte viability.

363 Previous study has shown that overexpression of miR-223 decreased HDAC2 expression

364 (Leuenberger et al. 2016). Silencing HDAC2 has been proved to reduce STAT3 phosphorylation,

365 while STAT3 phosphorylation could affect the pathological process associated with cell

366 ferroptosis (Pang et al. 2011; Qiang et al. 2020). Therefore, we hypothesized that miR-223-3p may

367 affect podocyte ferroptosis in HBV-GN through the regulation of STAT3 phosphorylation by

368 HDAC2. However, the specific mechanism needs further study. However, one limitation of our

369 study was the lack of animal experimental verification. In addition, there was no significant

370 statistical difference in SLC7A11 expression at the mRNA level after the treatment of the miR-

371 223-3p inhibitor, though corresponding protein expression was memorably reduced ($p<0.001$).

372 The mismatching of transcript expression data and protein expression data may be caused by the

373 following aspects: first, gene transcription and translation exist in time and site spacing; second,

374 there will be corresponding processing or modification after transcription and translation; third,

375 mRNA and protein own different half-lives, so the detection time may also affect the final data;

376 fourth, there may be a certain amount of protein reserves in cells that do not function.

377

378 **Conclusion**

379   In conclusion, our findings demonstrated that HBx overexpression induces podocyte ferroptosis

380   and plays a crucial role in the course of HBV-GN. BMSC-derived exosomes protect podocytes

381   from HBx-induced ferroptosis, and the main point is the delivery of miR-223-3p by exosomes.

382   This provides a new research direction for the cognition and treatment of HBV-GN.

383

384

385

386

387   **References**

388   Bochon B, Kozubska M, Surygala G, Witkowska A, Kuzniewicz R, Grzeszczak W, and Wystrychowski G. 2019.
389   Mesenchymal Stem Cells-Potential Applications in Kidney Diseases. *Int J Mol Sci* 20.
390   10.3390/ijms20102462

391   Collaborators GBDHB. 2022. Global, regional, and national burden of hepatitis B, 1990-2019: a systematic analysis
392   for the Global Burden of Disease Study 2019. *Lancet Gastroenterol Hepatol* 7:796-829. 10.1016/S2468-
393   1253(22)00124-8

394   Cui Y, Zhang Y, Zhao X, Shao L, Liu G, Sun C, Xu R, and Zhang Z. 2021. ACSL4 exacerbates ischemic stroke by
395   promoting ferroptosis-induced brain injury and neuroinflammation. *Brain Behav Immun* 93:312-321.
396   10.1016/j.bbi.2021.01.003

397   Ding C, Ding X, Zheng J, Wang B, Li Y, Xiang H, Dou M, Qiao Y, Tian P, and Xue W. 2020. miR-182-5p and miR-
398   378a-3p regulate ferroptosis in I/R-induced renal injury. *Cell Death & Disease* 11:929. 10.1038/s41419-020-
399   03135-z

400   Fu B, Ji Y, Hu S, Ren T, Bhuva MS, Li G, and Yang H. 2020. Efficacy and safety of anti-viral therapy for Hepatitis
401   B virus-associated glomerulonephritis: A meta-analysis. *Plos One* 15:e0227532.
402   10.1371/journal.pone.0227532

403   Gan B. 2021. Mitochondrial regulation of ferroptosis. *Journal of Cell Biology* 220. 10.1083/jcb.202105043

404   Guan Y, Liang X, Ma Z, Hu H, Liu H, Miao Z, Linkermann A, Hellwege JN, Voight BF, and Susztak K. 2021. A
405   single genetic locus controls both expression of DPEP1/CHMP1A and kidney disease development via
406   ferroptosis. *Nat Commun* 12:5078. 10.1038/s41467-021-25377-x

407   He P, Liu D, Zhang B, Zhou G, Su X, Wang Y, Li D, and Yang X. 2017. Hepatitis B Virus X Protein Reduces
408   Podocyte Adhesion via Downregulation of alpha3beta1 Integrin. *Cell Physiol Biochem* 41:689-700.
409   10.1159/000458428

410   Hiramatsu-Asano S, Sunahori-Watanabe K, Zeggar S, Katsuyama E, Mukai T, Morita Y, and Wada J. 2020. Deletion
411   of Mir223 Exacerbates Lupus Nephritis by Targeting S1pr1 in Fas(lpr/lpr) Mice. *Front Immunol* 11:616141.

412   10.3389/fimmu.2020.616141

413   Hu R, Quan S, Wang Y, Zhou Y, Zhang Y, Liu L, Zhou XJ, and Xing G. 2020. Spectrum of biopsy proven renal
414   diseases in Central China: a 10-year retrospective study based on 34,630 cases. *Sci Rep* 10:10994.
415   10.1038/s41598-020-67910-w

416   Hui D, Yan X, Wei J, Ruixia M, and Guangju G. 2014. Significance of mutations in hepatitis B virus X gene for the
417   pathogenesis of HB-associated glomerulonephritis. *Acta Virol* 58:278-281. 10.4149/av_2014_03_278

418   Jin J, Shi Y, Gong J, Zhao L, Li Y, He Q, and Huang H. 2019. Exosome secreted from adipose-derived stem cells
419   attenuates diabetic nephropathy by promoting autophagy flux and inhibiting apoptosis in podocyte. *Stem Cell*
420   *Res Ther* 10:95. 10.1186/s13287-019-1177-1

421   Jin J, Wang Y, Zheng D, Liang M, and He Q. 2022. A Novel Identified Circular RNA,
422   mmu_mmu_circRNA_0000309, Involves in Germacrone-Mediated Improvement of Diabetic Nephropathy
423   Through Regulating Ferroptosis by Targeting miR-188-3p/GPX4 Signaling Axis. *Antioxid Redox Signal*
424   36:740-759. 10.1089/ars.2021.0063

425   Kajarabille N, and Latunde-Dada GO. 2019. Programmed Cell-Death by Ferroptosis: Antioxidants as Mitigators. *Int*
426   *J Mol Sci* 20. 10.3390/ijms20194968

427   Kuo CY, Chiu V, Hsieh PC, Huang CY, Huang SJ, Tzeng IS, Tsai FM, Chen ML, Liu CT, and Chen YR. 2020.
428   Chrysophanol attenuates hepatitis B virus X protein-induced hepatic stellate cell fibrosis by regulating
429   endoplasmic reticulum stress and ferroptosis. *J Pharmacol Sci* 144:172-182. 10.1016/j.jphs.2020.07.014

430   Lei XY, Chen XX, Sun YH, Gao MD, Hu XX, and Suo YH. 2019. Hepatitis B virus X protein decreases nephrin
431   expression and induces podocyte apoptosis via activating STAT3. *Experimental and Therapeutic Medicine*
432   17:4223-4229. 10.3892/etm.2019.7453

433   Leuenberger C, Schuoler C, Bye H, Mignan C, Rechsteiner T, Hillinger S, Opitz I, Marsland B, Faiz A, Hiemstra PS,
434   Timens W, Camici GG, Kohler M, Huber LC, and Brock M. 2016. MicroRNA-223 controls the expression
435   of histone deacetylase 2: a novel axis in COPD. *J Mol Med (Berl)* 94:725-734. 10.1007/s00109-016-1388-1

436   Li B, Li Y, Li S, Li H, Liu L, and Xu Y. 2022. Inhibition of Protease Activated Receptor 2 Attenuates HBx-Induced
437   Inflammation and Mitochondria Oxidative Stress. *Infect Drug Resist* 15:961-973. 10.2147/IDR.S343864

438   Li J, Cao F, Yin HL, Huang ZJ, Lin ZT, Mao N, Sun B, and Wang G. 2020a. Ferroptosis: past, present and future.
439   *Cell Death & Disease* 11:88. 10.1038/s41419-020-2298-2

440   Li X, Liao J, Su X, Li W, Bi Z, Wang J, Su Q, Huang H, Wei Y, Gao Y, Li J, Liu L, and Wang C. 2020b. Human
441   urine-derived stem cells protect against renal ischemia/reperfusion injury in a rat model via exosomal miR-
442   146a-5p which targets IRAK1. *Theranostics* 10:9561-9578. 10.7150/thno.42153

443   Lin F, Chen W, Zhou J, Zhu J, Yao Q, Feng B, Feng X, Shi X, Pan Q, Yu J, Li L, and Cao H. 2022. Mesenchymal
444   stem cells protect against ferroptosis via exosome-mediated stabilization of SLC7A11 in acute liver injury.
445   *Cell Death & Disease* 13:271. 10.1038/s41419-022-04708-w

446   Liu GZ, Xu XW, Tao SH, Gao MJ, and Hou ZH. 2021a. HBx facilitates ferroptosis in acute liver failure via EZH2
447   mediated SLC7A11 suppression. *J Biomed Sci* 28:67. 10.1186/s12929-021-00762-2

448   Liu Y, Shi C, Fan J, Wang B, and Li G. 2020. Hepatitis B-related glomerulonephritis and optimization of treatment.
449   *Expert Rev Gastroenterol Hepatol* 14:113-125. 10.1080/17474124.2020.1717948

450   Liu Y, Zhang S, Xue Z, Zhou X, Tong L, Liao J, Pan H, and Zhou S. 2021b. Bone mesenchymal stem cells-derived
451   miR-223-3p-containing exosomes ameliorate lipopolysaccharide-induced acute uterine injury via interacting
452   with endothelial progenitor cells. *Bioengineered* 12:10654-10665. 10.1080/21655979.2021.2001185

453 Lu FB, Chen DZ, Chen L, Hu ED, Wu JL, Li H, Gong YW, Lin Z, Wang XD, Li J, Jin XY, Xu LM, and Chen YP.
454   2019. Attenuation of Experimental Autoimmune Hepatitis in Mice with Bone Mesenchymal Stem Cell-
455   Derived Exosomes Carrying MicroRNA-223-3p. *Mol Cells* 42:906-918. 10.14348/molcells.2019.2283

456 Mao RY, Shen JN, and Hu XL. 2021. BMSCs-derived exosomal microRNA-let-7a plays a protective role in diabetic
457   nephropathy via inhibition of USP22 expression. *Life Sciences* 268. 10.1016/j.lfs.2020.118937

458 Mishima E, Sato E, Ito J, Yamada KI, Suzuki C, Oikawa Y, Matsuhashi T, Kikuchi K, Toyohara T, Suzuki T, Ito S,
459   Nakagawa K, and Abe T. 2020. Drugs Repurposed as Antiferroptosis Agents Suppress Organ Damage,
460   Including AKI, by Functioning as Lipid Peroxyl Radical Scavengers. *J Am Soc Nephrol* 31:280-296.
461   10.1681/ASN.2019060570

462 Nikfarjam S, Rezaie J, Zolbanin NM, and Jafari R. 2020. Mesenchymal stem cell derived-exosomes: a modern
463   approach in translational medicine. *J Transl Med* 18:449. 10.1186/s12967-020-02622-3

464 Pang M, Ma L, Liu N, Ponnusamy M, Zhao TC, Yan H, and Zhuang S. 2011. Histone deacetylase 1/2 mediates
465   proliferation of renal interstitial fibroblasts and expression of cell cycle proteins. *Journal of Cellular
466   Biochemistry* 112:2138-2148. 10.1002/jcb.23135

467 Qiang Z, Dong H, Xia Y, Chai D, Hu R, and Jiang H. 2020. Nrf2 and STAT3 Alleviates Ferroptosis-Mediated IIR-
468   ALI by Regulating SLC7A11. *Oxidative Medicine and Cellular Longevity* 2020:5146982.
469   10.1155/2020/5146982

470 Song Y, Wang B, Zhu X, Hu J, Sun J, Xuan J, and Ge Z. 2021. Human umbilical cord blood-derived MSCs exosome
471   attenuate myocardial injury by inhibiting ferroptosis in acute myocardial infarction mice. *Cell Biol Toxicol*
472   37:51-64. 10.1007/s10565-020-09530-8

473 Wang Y, Quan F, Cao Q, Lin Y, Yue C, Bi R, Cui X, Yang H, Yang Y, Birnbaumer L, Li X, and Gao X. 2021.
474   Quercetin alleviates acute kidney injury by inhibiting ferroptosis. *J Adv Res* 28:231-243.
475   10.1016/j.jare.2020.07.007

476 Wu L, Tian X, Zuo H, Zheng W, Li X, Yuan M, Tian X, and Song H. 2022a. miR-124-3p delivered by exosomes
477   from heme oxygenase-1 modified bone marrow mesenchymal stem cells inhibits ferroptosis to attenuate
478   ischemia-reperfusion injury in steatotic grafts. *J Nanobiotechnology* 20:196. 10.1186/s12951-022-01407-8

479 Wu WY, Wang ZX, Li TS, Ding XQ, Liu ZH, Yang J, Fang L, and Kong LD. 2022b. SSBP1 drives high fructose-
480   induced glomerular podocyte ferroptosis via activating DNA-PK/p53 pathway. *Redox Biol* 52:102303.
481   10.1016/j.redox.2022.102303

482 Xu S, He Y, Lin L, Chen P, Chen M, and Zhang S. 2021. The emerging role of ferroptosis in intestinal disease. *Cell
483   Death & Disease* 12:289. 10.1038/s41419-021-03559-1

484 Yang Y, Wang X, Zhang Y, and Yuan W. 2018. Hepatitis B virus X protein and proinflammatory cytokines synergize
485   to enhance TRAIL-induced apoptosis of renal tubular cells by upregulation of DR4. *Int J Biochem Cell Biol*
486   97:62-72. 10.1016/j.biocel.2018.02.006

487 Yang YT, Wang X, Zhang YY, and Yuan WJ. 2019. The histone demethylase LSD1 promotes renal inflammation by
488   mediating TLR4 signaling in hepatitis B virus-associated glomerulonephritis. *Cell Death & Disease* 10:278.
489   10.1038/s41419-019-1514-4

490 Yi X, and Tang X. 2021. Exosomes From miR-19b-3p-Modified ADSCs Inhibit Ferroptosis in Intracerebral
491   Hemorrhage Mice. *Front Cell Dev Biol* 9:661317. 10.3389/fcell.2021.661317

492 Zhang G, Zou X, Huang Y, Wang F, Miao S, Liu G, Chen M, and Zhu Y. 2016. Mesenchymal Stromal Cell-Derived
493   Extracellular Vesicles Protect Against Acute Kidney Injury Through Anti-Oxidation by Enhancing

494   Nrf2/ARE Activation in Rats. *Kidney Blood Press Res* 41:119-128. 10.1159/000443413

495   Zhang Q, Hu Y, Hu JE, Ding Y, Shen Y, Xu H, Chen H, and Wu N. 2021. Sp1-mediated upregulation of Prdx6

496   expression prevents podocyte injury in diabetic nephropathy via mitigation of oxidative stress and ferroptosis.

497   *Life Sci* 278:119529. 10.1016/j.lfs.2021.119529

498   Zhao Y, Gan Y, Xu G, Hua K, and Liu D. 2020. Exosomes from MSCs overexpressing microRNA-223-3p attenuate

499   cerebral ischemia through inhibiting microglial M1 polarization mediated inflammation. *Life Sci*

500   260:118403. 10.1016/j.lfs.2020.118403

501

502

503

504

505

506

507

508

509

510

511

512

513

514

Table1: Antibodies list

N

Manuscript to be reviewed/

2 **Table 1**: Antibodies list

Antibody	Vendor	Catalog no.	Working dilution
GPX4	Proteintech	14432-1-AP	1:1000
SLC7A11	Proteintech	26864-1-AP	1:1000
ACSL4	ABclonal	A6826	1:1000
CD9	Abcam	ab92726	1:1000
TSG101	Abcam	ab125011	1:1000
Calnexin	Abcam	ab22595	1:1000
GAPDH	Proteintech	60004-1-Ig	1:5000

3 GPX4: glutathione peroxidase 4; SLC7A11: solute carrier family 7 member 11; ACSL4: acyl-CoA

4 synthetase long-chain family member 4.

PeerJ reviewing PDF | (2022:12:80295:2:0:NEW 1 Apr 2023)

Table 2: Primers list

2 **Table 2**: Primers list

Gene	Primer sequence (5′-3′)
GPX4	F, GCTGGACGAGGGGAGGAG
	R, GGAAAACTCGTGCATGGAGC
SLC7A11	F, TCTCCAAAGGAGGTTACCTGC
	R, AGACTCCCCTCAGTAAAGTGAC
ACSL4	F, ACTGGCCGACCTAAGGGAG
	R, GCCAAAGGCAAGTAGCCAATA
GAPDH	F, AGAAGGCTGGGGCTCATTTG
	R, AGGGGCCATCCACAGTCTTC
U6	F, GCTCGCTTCGGCAGCACA
	R, GAACGCTTCACGAATTTGCGTG

3 F: forward; R: reverse.

Figure 1

HBx overexpression induced podocytes ferroptosis.

A, the cell viability of podocytes as detected by CCK-8 assay. B, the concentration of iron in podocytes. C, the concentration of MDA in podocytes. D, the ROS generation as detected by flow cytometry. E, the protein expression of ferroptosis related proteins (GPX4, ACSL4, SLC7A11) in podocytes as detected by Western blot analysis, normalized to GAPDH. F, the mRNA expression of GPX4, ACSL4, SLC7A11 in podocytes as detected by qRT-PCR. The experiment was repeated three times. Control: podocytes without any transfection, Lenti-NC: podocytes transfected with negative control lentivirus, Lenti-HBx: podocytes transfected with HBx overexpression lentivirus. *, $p<0.05$, **, $p<0.01$, ***, $p<0.001$ versus Control or Lenti-NC.

A

B

C

D

ROS

E

ACSL4   80 kDa
SLC7A11   55 kDa
GPX4   22kDa
GAPDH   36 kDa

F
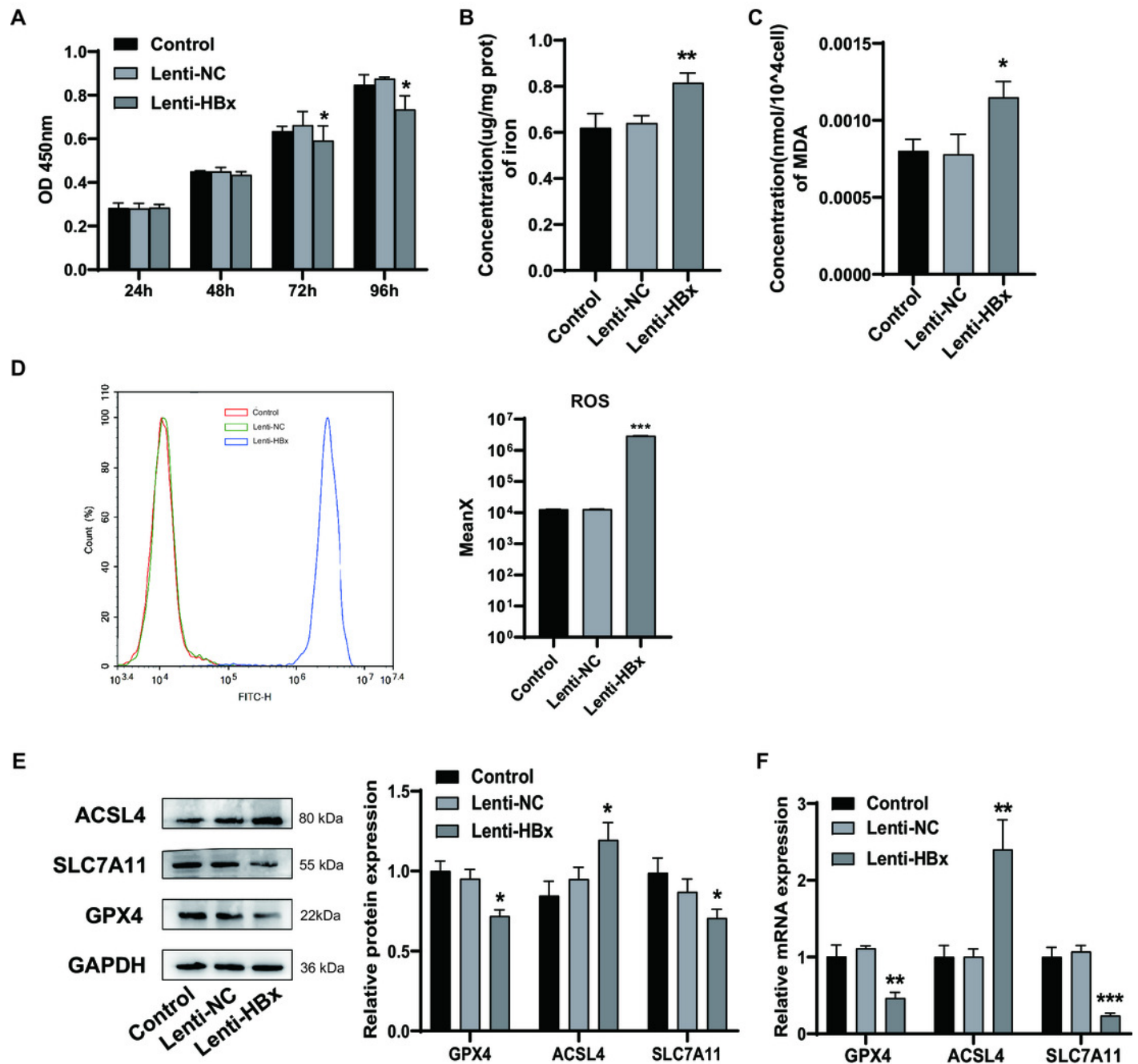
Figure 2

Characterization of exosomes isolated from BMSCs.

A, observation of morphology of exosomes by transmission EM (scale bar, 200nm). B, size distribution of BMSC-derived exosomes measured by NTA analysis. C, CD9, TSG101, and calnexin detected by Western blot analysis. CL: positive control, Exo: exosomes.
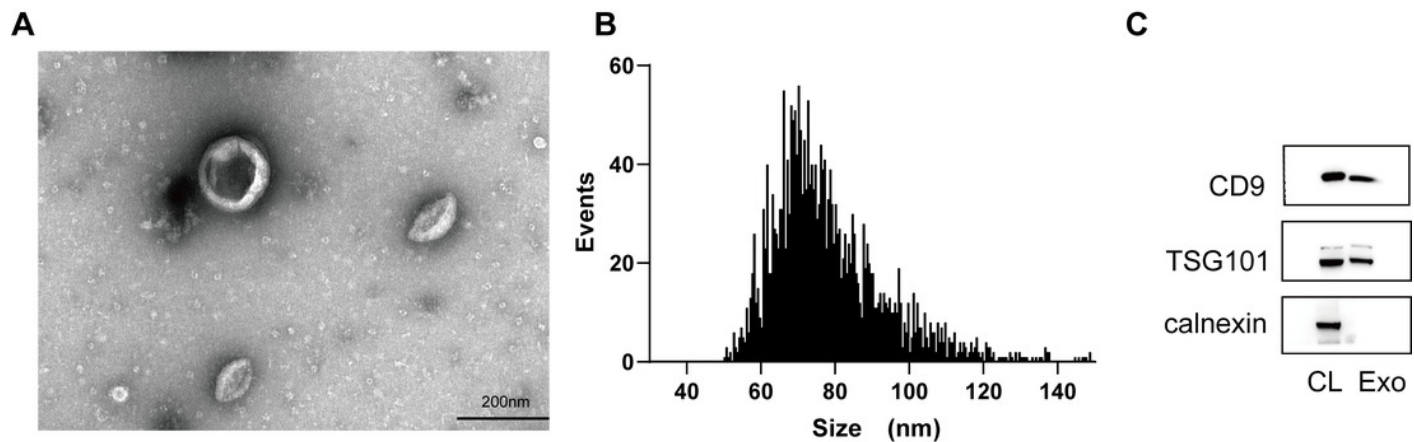
Figure 3

BMSC-derived exosomes inhibited podocyte ferroptosis induced by HBx.

A, differential interference contrast (DIC) microscopy image and fluorescence microscopy image taken by laser scanning confocal microscope (scale bar 25μm,24h). Red fluorescence PKH26 used to label BMSC-derived exosomes. Uptake efficiency of PKH26-labeled exosomes by podocytes. B, the cell viability of podocytes as detected by CCK-8 assay. C, the concentration of Fe in podocytes. D, the concentration of MDA in podocytes. E, the ROS generation as detected by flow cytometry. F, the protein expression of ferroptosis related proteins (GPX4, ACSL4, SLC7A11) in podocytes as detected by Western blot analysis, normalized to GAPDH. G, the mRNA expression of GPX4, ACSL4, SLC7A11 in podocytes as detected by qRT-PCR. The experiment was repeated three times. Control: podocytes without any transfection, Lenti-NC: podocytes transfected with negative control lentivirus, Lenti-HBx: podocytes transfected with HBx overexpression lentivirus, Lenti-HBx+exo: podocytes treated with exosomes after transfected with HBx overexpression lentivirus. *, $p<0.05$, **, $p<0.01$, ***, $p<0.001$ versus Control or Lenti-NC. #, $p<0.05$, ##, $p<0.01$, ###, $p<0.001$ versus Lenti-HBx.
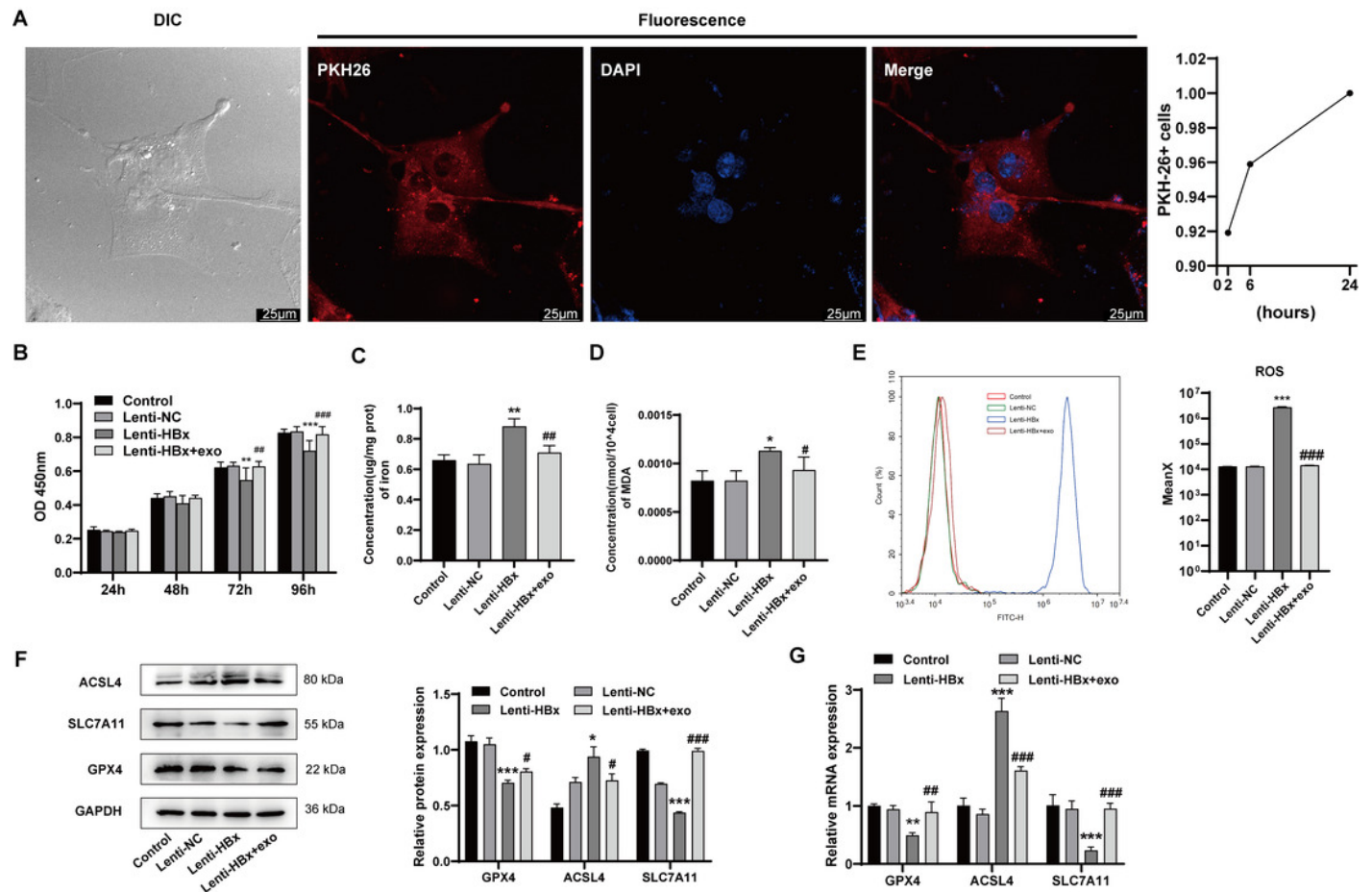
Figure 4

Exosomes from BMSCs delivered miR-223-3p to suppress HBx-induced ferroptosis in podocytes.

A, the expression of miR-223-3p as detected by qRT-PCR. B, the cell viability of podocytes as detected by CCK-8 assay. C, the concentration of iron in podocytes. D, the concentration of MDA in podocytes. E-F, the ROS generation as detected by flow cytometry. G, the protein expression of ferroptosis related proteins (GPX4, ACSL4, SLC7A11) in podocytes as detected by Western blot analysis, normalized to GAPDH. H, the mRNA expression of GPX4, ACSL4, SLC7A11 in podocytes as detected by qRT-PCR. The experiment was repeated three times. Control: podocytes without any transfection, HBx: podocytes transfected with HBx overexpression lentivirus, HBx+exo: podocytes treated with exosomes after transfected with HBx overexpression lentivirus, HBx+exo+inhibitor NC: podocytes treated with exosomes and negative control miRNA inhibitor after transfected with HBx overexpression lentivirus, HBx+exo+miR-223-3p inhibitor: podocytes treated with exosomes and miR-223-3p inhibitor after transfected with HBx overexpression lentivirus. ***, $p<0.001$ versus Control. #, $p<0.05$, ##, $p<0.01$, ###, $p<0.001$ versus HBx. &, $p<0.05$, &&, $p<0.01$, &&&, $p<0.001$ versus HBx+exo+inhibitor NC.